Electronic Supporting Information

Switchable coordination bonds in 3D cyano-bridged perovskite ferroelastics: Achieving the largest leap of symmetry breaking and enhanced dielectric switching performance

*Sheng-qian Hu, Meng-zhen Li, Zhao-hong Chen, Jun-Si Zhou, Luan-Ying Ji, Yong Ai and Xiao-Gang Chen**

Experimental Section

Preparation of FAZT-K. All chemicals were commercially available and were used without further purification. 3-fluoroazetidine hydrochloride (1.6731 g, 15 mmol) was added to 20 ml aqueous solution of $K_3Fe(CN)_6$ (1.6463 g, 5 mmol). The solution was placed in a fume hood with tin foil wrapped to avoid light treatment. After slowly evaporating at room temperature for ten days, we obtained reddish-brown block crystals FAZT-K.

Preparation of AZT-K. All chemicals were commercially available and were used without further purification. Azetidine hydrochloride (1.4034 g, 15 mmol) was added to 70 ml aqueous solution of $K_3Fe(CN)_6$ (1.6463 g, 5 mmol). The solution was placed in a fume hood with tin foil wrapped to avoid light treatment. After slowly evaporating at room temperature for over 3 weeks, we obtained reddish-brown block crystals AZT-K.

Preparation of FAZT-Rb. All chemicals except $Ag_3Fe(CN)_6$ were commercially available and were used without further purification. $Ag_3Fe(CN)_6$ is obtained by collecting the filter residue after the reaction of $K_3Fe(CN)_6$ and silver nitrate in the

aqueous solution. 3-fluoroazetidine hydrochloride (1.6731 g, 15 mmol) was added to the solution of $Rb_3Fe(CN)_6$ which is obtained by filtration after the reaction of $Ag_3Fe(CN)_6$ (2.6778 g, 5 mmol) and rubidium chloride (1.8138 g, 15 mmol) in 20 ml aqueous solution. The solution was placed in a fume hood with tin foil wrapped to avoid light treatment. After slowly evaporating at room temperature for ten days, we obtained reddish-brown block crystals FAZT-Rb.

Preparation of AZT-Rb. All chemicals except $Ag_3Fe(CN)_6$ were commercially available and were used without further purification. $Ag_3Fe(CN)_6$ is obtained by collecting the filter residue after the reaction of $K_3Fe(CN)_6$ and silver nitrate in the aqueous solution. Azetidine hydrochloride (1.4034 g, 15 mmol) was added to the solution of $Rb_3Fe(CN)_6$ which is obtained by filtration after the reaction of $Ag_3Fe(CN)_6$ (2.6778 g, 5 mmol), and rubidium chloride (1.8138 g, 15 mmol) in 20 ml aqueous solution. The solution was placed in a fume hood with tin foil wrapped to avoid light treatment. After slowly evaporating at room temperature for eight days, we obtained reddish-brown block crystals AZT-Rb.

Preparation of FAZT-Cs. All chemicals except $Ag_3Fe(CN)_6$ were commercially available and were used without further purification. $Ag_3Fe(CN)_6$ is obtained by collecting the filter residue after the reaction of $K_3Fe(CN)_6$ and silver nitrate in the aqueous solution. 3-fluoroazetidine hydrochloride (1.673 g, 15 mmol) was added to the solution of $Cs_3Fe(CN)_6$ which is obtained by filtration after the reaction of $Ag_3Fe(CN)_6$ (2.6778 g, 5 mmol) and cesium chloride (2.5354 g, 15 mmol) in 20 ml aqueous solution. The solution was placed in a fume hood with tin foil wrapped to avoid light treatment.

After slowly evaporating at room temperature for eight days, we obtained reddish-brown block crystals FAZT-Cs.

Preparation of AZT-Cs. All chemicals except $Ag_3Fe(CN)_6$ were commercially available and were used without further purification. $Ag_3Fe(CN)_6$ is obtained by collecting the filter residue after the reaction of $K_3Fe(CN)_6$ and silver nitrate in the aqueous solution. Azetidine hydrochloride (1.4034 g, 15 mmol) was added to the solution of $Cs_3Fe(CN)_6$ which is obtained by filtration after the reaction of $Ag_3Fe(CN)_6$ (2.6778 g, 5 mmol) and cesium chloride (2.5354 g, 15 mmol) in 20 ml aqueous solution. The solution was placed in a fume hood with tin foil wrapped to avoid light treatment. After slowly evaporating at room temperature for a week, we obtained reddish-brown block crystals AZT-Cs.

Characterizations:

TGA measurements: About 5 mg of dried and ground powder is placed in a small crucible to make a sample. The thermal stability of samples was investigated on a Perkin Elmer TGA8000 thermal gravimetric analyzer with a rate of 40 K/min. The measurement temperature range was from 300 K to 873 K.

Powder X-ray diffraction: The dried and ground powder was filled into the groove of the glass slide to make a sample. Room-temperature powder X-ray diffraction (PXRD) data were collected by using a Rigaku D/MAX 2000 PC X-ray diffraction system with Cu Kα radiation in the 2θ range of 10 °-50 ° with a step size of 0.02 °, and the scan speed is 10 °/min.

DSC measurements: About 5 mg of dried and ground powder is placed in an aluminum crucible to make a sample. Differential scanning calorimetry (DSC) measurements were recorded on a Perkin-Elmer Diamond DSC instrument by heating and cooling powder samples with a rate of 20 K/min in a nitrogen atmosphere.

Dielectric measurements: The samples were made with pressed powder pellets with a thickness of about 4 mm. The samples were coated with silver conducting glue on both sides with an area of about 12 mm^2. The samples were fixed on the hexagonal electrode by copper wires which were stuck on both sides of the samples with silver glue. Dielectric measurements were measured with a TH2828A impedance analyzer at 1 MHz. The heating and cooling rate was about 6 K/min, the applied voltage was 1V. For dielectric switching measurements, the response time of one dielectric switch is about 15 minutes, and the total cycle time is about 80 minutes.

Single crystal X-ray crystallography: The transparent crack-free single crystal was selected as the measurement sample under the microscope. Single-crystal X-ray diffraction measurements of all compounds were performed on the Rigaku XtaLAB Synergy-DW diffractometer with Cu-Kα radiation (λ = 1.54184 Å) at various temperatures. Rigaku Crystal Clear 1.3.5 was used for data collection, cell refinement, and data reduction.

Optical microscopy measurements: A thin film was obtained by evaporating 20 μL of 10 mg/mL of aqueous solution of the measured compounds on sheet glass with an area of 1 cm^2 on a hot stage of 323 K. Ferroelastic domain observations were carried out

using an OLYMPUS BX53-P polarizing microscope. The temperature was controlled by a Linkam LTS420 cooling/heating stage with a rate of 10 K/min.

[CCDC 2352607-2352619 contains the supplementary crystallographic data for this paper. These data can be obtained free of charge from The Cambridge Crystallographic Data Centre via www.ccdc.cam.ac.uk/data_request/cif.]

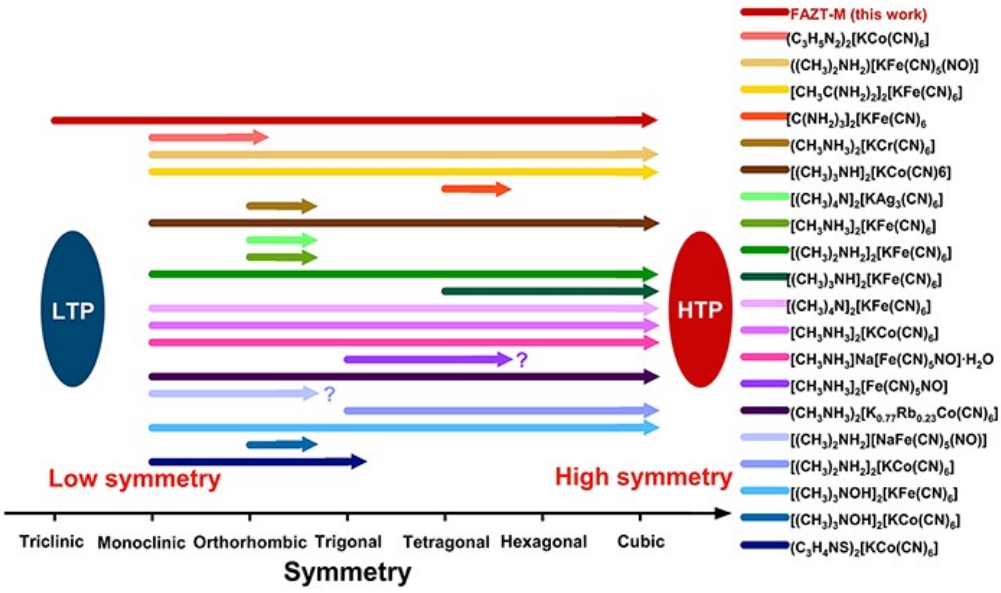

Figure S1. Symmetry change of FAZT-M between LTP and HTP compare to other 3D cyano-bridged perovskites.

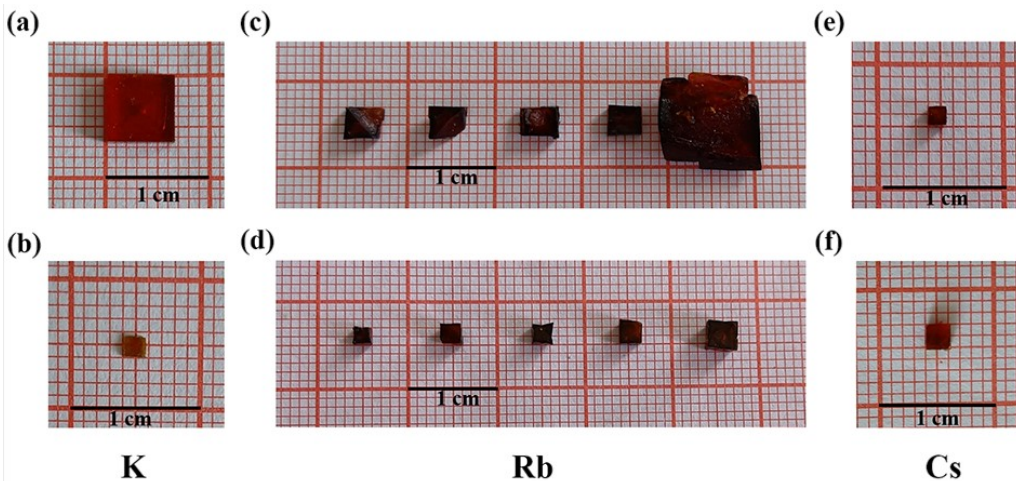

Figure S2. Crystal morphology of FAZT-K (a), AZT-K (b), FAZT-Rb (c), AZT-Rb (d), FAZT-Cs (e) and AZT-Cs (f).

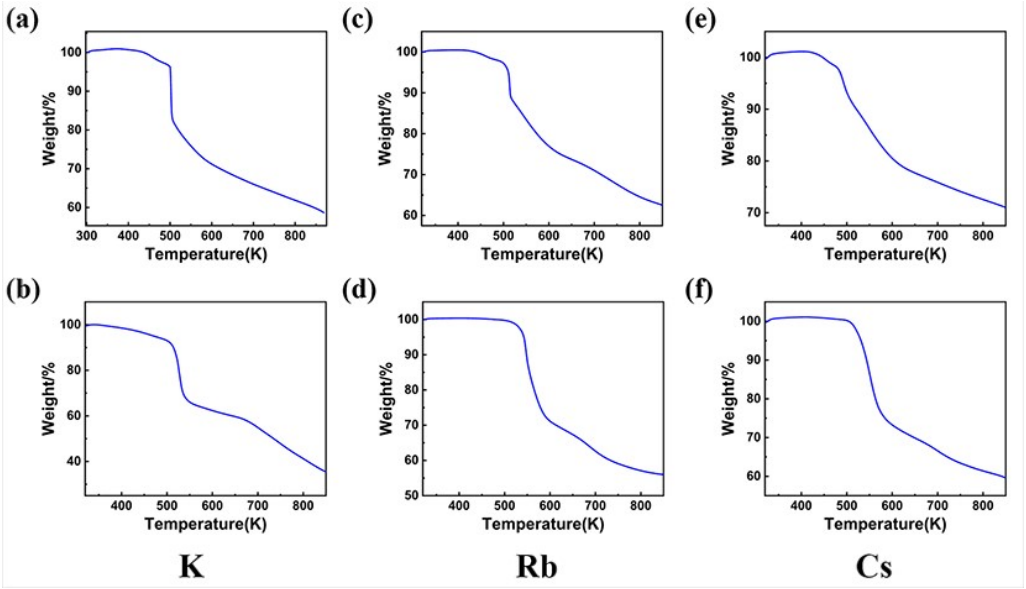

Figure S3. TGA curves of FAZT-K (a), AZT-K (b), FAZT-Rb (c), AZT-Rb (d), FAZT-Cs (e) and AZT-Cs (f).

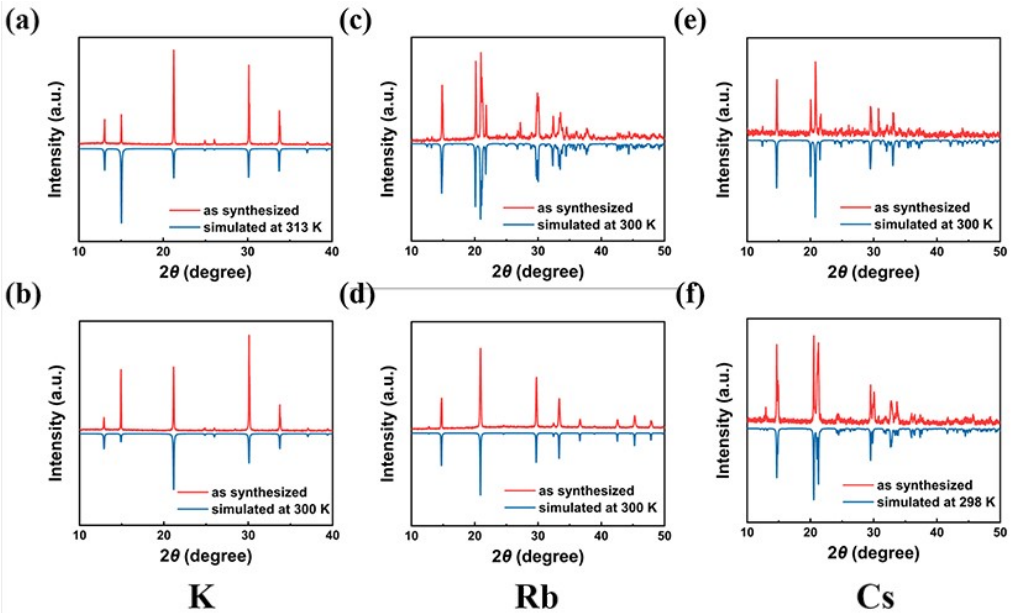

Figure S4. The PXRD patterns confirmed the phase purity of the as-synthesized sample for FAZT-K (a), AZT-K (b), FAZT-Rb (c), AZT-Rb (d), FAZT-Cs (e) and AZT-Cs (f).

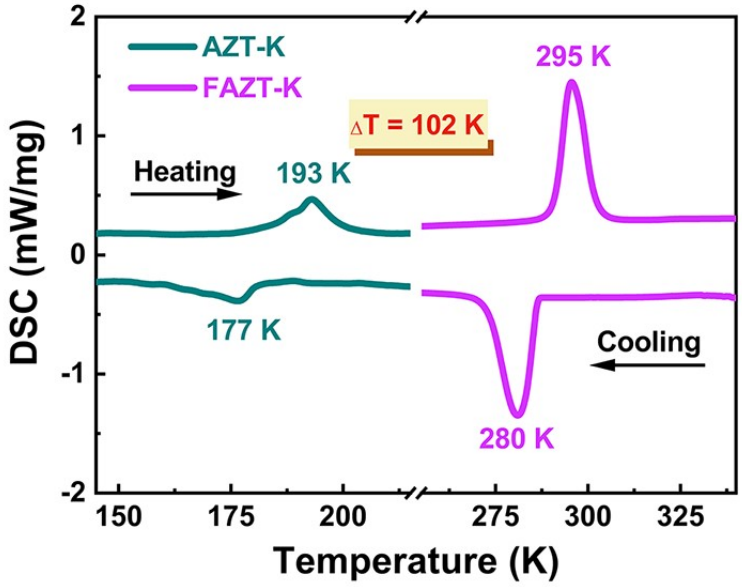

Figure S5. DSC curves of FAZT-K and AZT-K.

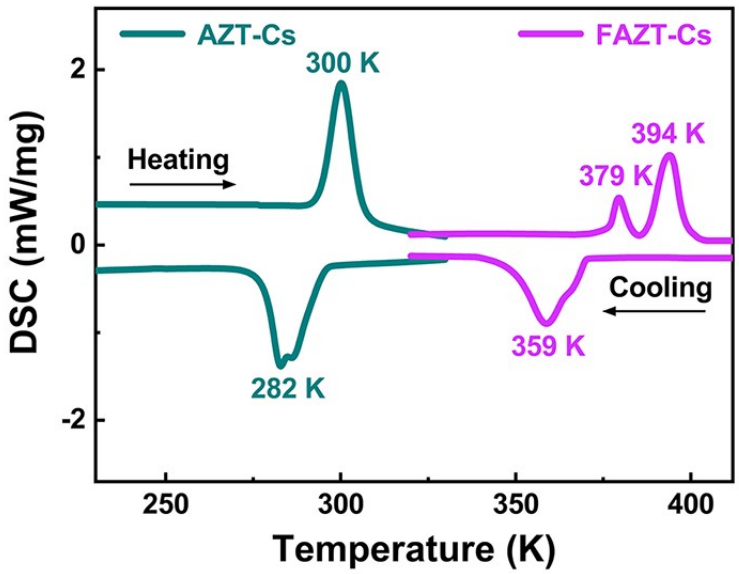

Figure S6. DSC curves of FAZT-Cs and AZT-Cs.

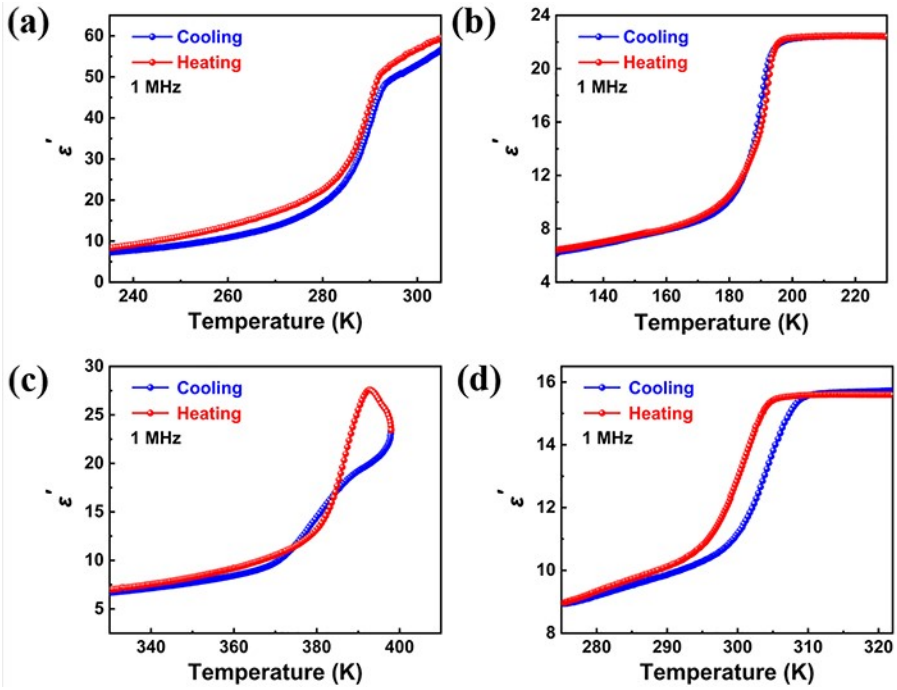

Figure S7. Temperature-dependent dielectric constants of FAZT-K (a), AZT-K (b), FAZT-Cs (c), and AZT-Cs (d).

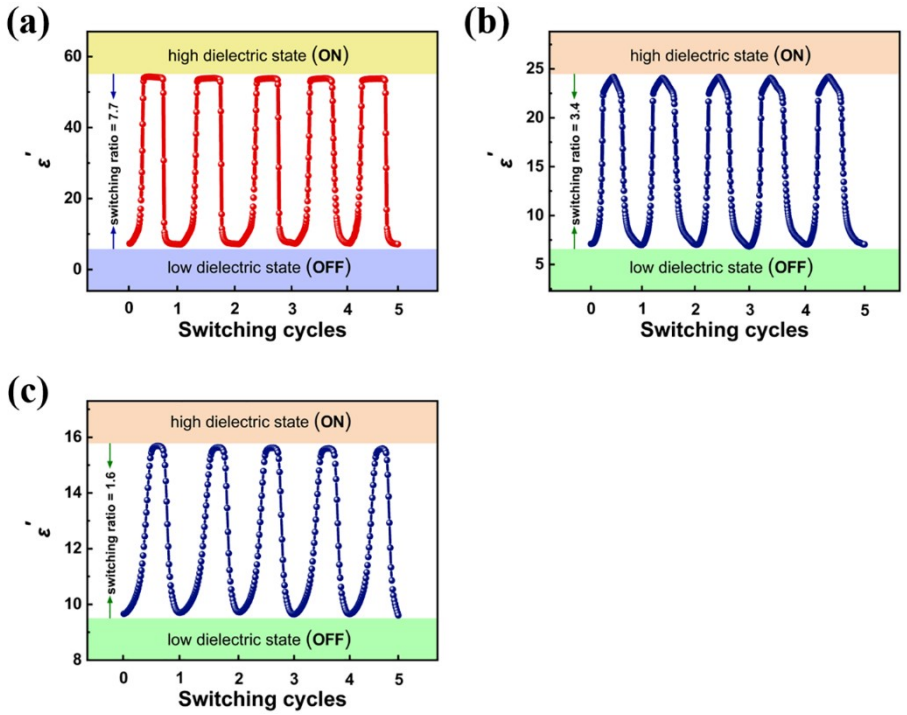

Figure S8. Reversible dielectric switching (ON and OFF) of ε' between HTP and LTP measured for FAZT-K (a), AZT-K (b), and AZT-Cs (c) at 1 MHz.

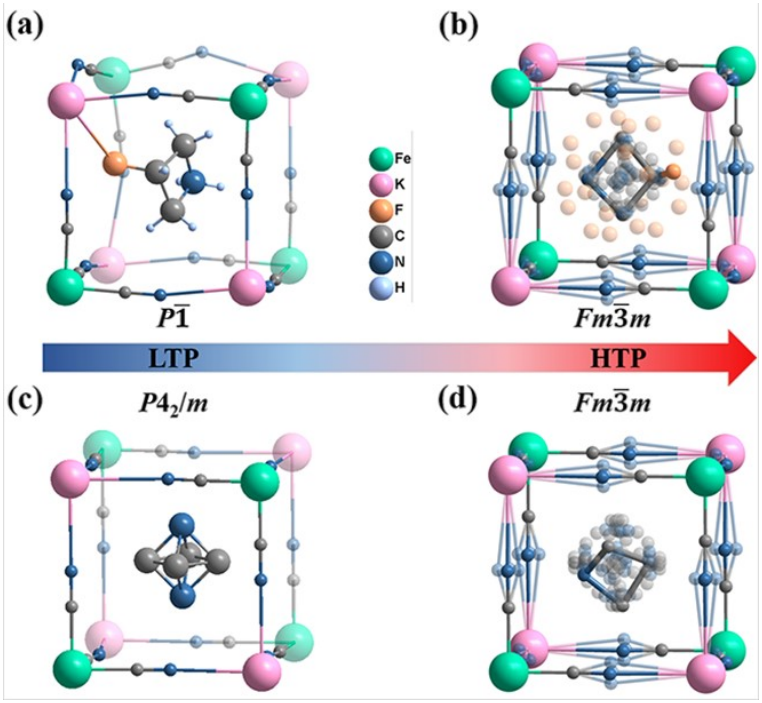

Figure S9. Crystal structures of FAZT-K and AZT-K. The basic unit of the framework in LTP and HTP of FAZT-K (a), (b), and AZT-K (c), (d). The hydrogen atoms in the HTP and of AZT-K in the LTP are omitted for clarity.

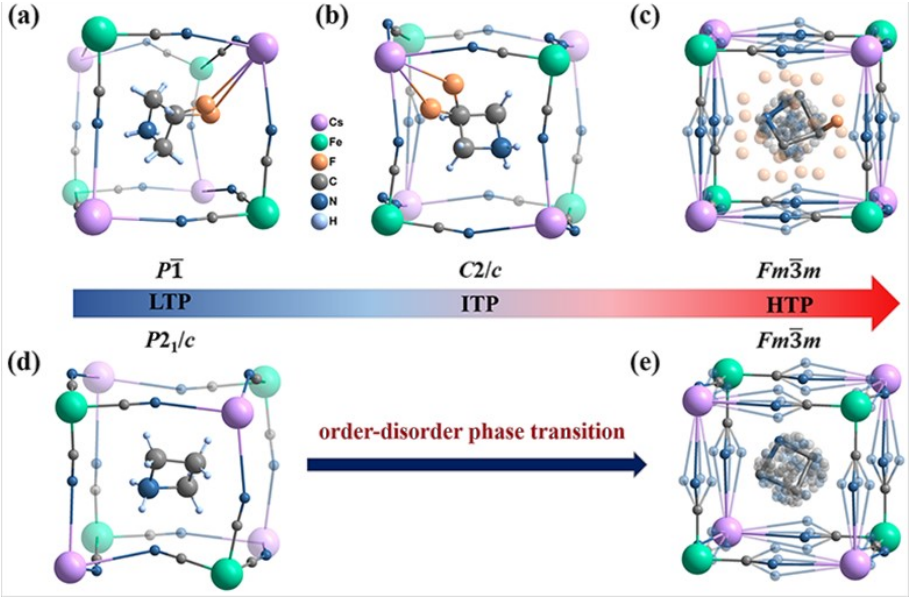

Figure S10. Crystal structures of FAZT-Cs and AZT-Cs. The basic unit of the framework in LTP, ITP, and HTP of FAZT-Cs (a), (b), (c), and AZT-Cs (d), (e). The hydrogen atoms in the HTP are omitted for clarity.

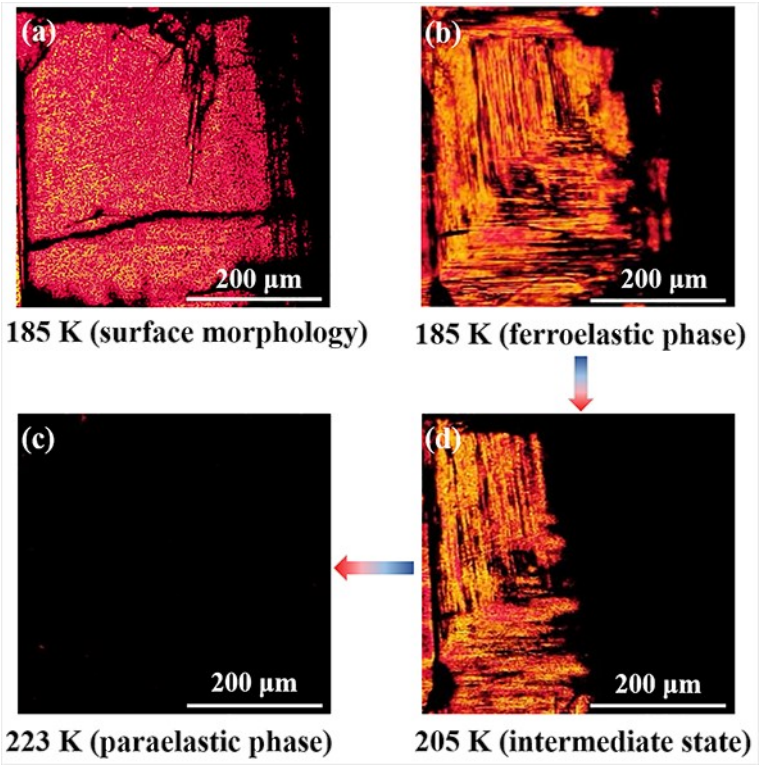

Figure S11. Evolution of ferroelastic domains between the ferroelastic phase and paraelastic phase for AZT-Rb.

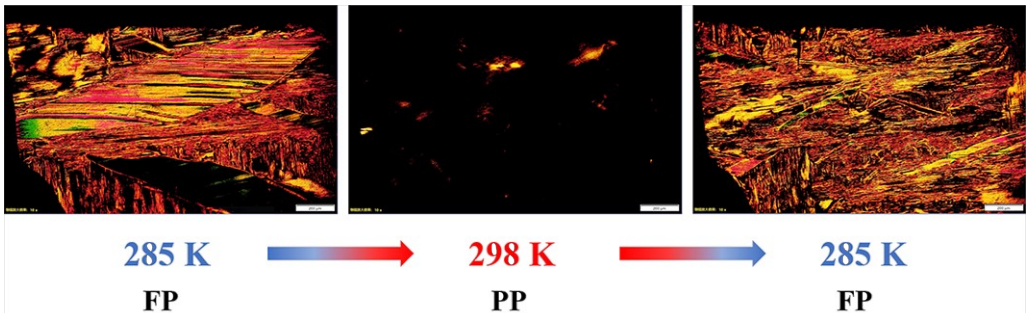

Figure S12. Evolution of ferroelastic domains repeatedly cycling between the ferroelastic phase (FP) and paraelastic phases (PP) for FAZT-K.

Table S1. Space groups and T_c of other 3D cyano-bridged perovskites mentioned in Figure S1 in the HTP and LTP, respectively.

	space group in the LTP	**space group in the HTP**	**T_c / K**
$(C_5H_5N_2)_2[KCo(CN)_6]$[1]	$C2/c$	$R\bar{3}m$	110/198
$((CH3)_2NH_2)[KFe(CN)_5(NO)]$[2]	$P2_12_12_1$	$Pnma$	297
$[CH_3C(NH_2)_2]_2[KFe(CN)_6$[3]	$C2/m$	$Fm\bar{3}m$	201/385
$[C(NH_2)_3]_2[KFe(CN)_6]$[4]	$R\bar{3}c$	$Fm\bar{3}m$	411/439
$(CH_3NH_3)_2[KCr(CN)_6]$[5]	$C2/c$	?	450
$[(CH_3)_3NH]_2[KCo(CN)_6]$[6]	$C2/c$	$Fm\bar{3}m$	350
$[(CH_3)_4N]_2[KAg_3(CN)_6]$[7]	$R\bar{3}c$	?	?
$[CH_3NH_3]_2[KFe(CN)_6]$[8]	$C2/c$	$Fm\bar{3}m$	429
$[(CH_3)_2NH_2]_2[KFe(CN)_6]$[8]	$C2/c$	$Fm\bar{3}m$	226
$[(CH_3)_3NH]_2[KFe(CN)_6]$[8]	$C2/c$	$Fm\bar{3}m$	316
$[(CH_3)_4N]_2[KFe(CN)_6]$[8]	$I4/m$	$Fm\bar{3}m$	350
$[CH_3NH_3]_2[KCo(CN)_6]$[9]	$C2/c$	$Fm\bar{3}m$	421
$[CH_3NH_3]Na[Fe(CN)_5NO]\cdot H_2O$[10]	$Pbcm$	$Cmcm$	229/238
$[CH_3NH_3]_2[Fe(CN)_5NO]$[10]	$Pbcm$	$Cmcm$	207/211/223
$(CH_3NH_3)_2[K_{0.77}Rb_{0.23}Co(CN)_6]$[11]	$C2/c$	$Fm\bar{3}m$	435
$[(CH_3)_2NH_2][NaFe(CN)_5(NO)]$[12]	$Pna2_1$	$Pnma$	423
$[(CH_3)_2NH_2]_2[KCo(CN)_6]$[13]	$P4/mnc$	$P4/mnc$	245
$[(CH_3)_3NOH]_2[KFe(CN)_6]$[14]	Cc	$Fm\bar{3}m$	402
$[(CH_3)_3NOH]_2[KCo(CN)_6]$[15]	Cc	$Fm\bar{3}m$	417
$(C_3H_4NS)_2[KCo(CN)_6]$[16]	Monoclinic	$Cmcm$	210/237

Table S2. The crystal data for compounds FAZT-Rb and AZT-Rb at different temperatures.

	$[C_3H_6NHF]_2[RbFe(CN)_6]$		$[C_3H_6NH_2]_2[RbFe(CN)_6]$	
Formula weight	449.63	899.26	413.65	827.29
Temperature/K	300	373	173	300
Crystal system	triclinic	cubic	monoclinic	cubic
Space group	$P\bar{1}$	$Fm\bar{3}m$	$P2_1/c$	$Fm\bar{3}m$
a/Å	8.1709(6)	12.08650(10)	14.0338(4)	12.0140(2)
b/Å	8.5006(6)	12.08650(10)	8.5636(3)	12.0140(2)
c/Å	14.7072(5)	12.08650(10)	14.7882(4)	12.0140(2)
α/°	104.555(4)	90	90	90
β/°	90.341(5)	90	110.417(3)	90
γ/°	118.608(7)	90	90	90
Volume/Å^3	858.39(11)	1765.64(4)	1665.59(9)	1734.06(9)
Z	2	2	4	2
μ/mm^{-1}	10.780	10.482	10.873	3.667
ρ_{calc}/g ·cm^{-3}	1.740	1.691	1.650	1.584
R_{int}	0.0632	0.0324	0.0740	0.0153
R_1 [I>=2σ (I)]	0.0880	0.0313	0.0987	0.0263
wR_2 [I>=2σ (I)]	0.2616	0.0955	0.2774	0.0554
R_1 [all data]	0.0954	0.0313	0.1064	0.0282
wR_2 [all data]	0.2676	0.0955	0.2810	0.0564
Goodness-of-fit on F^2	1.080	1.168	1.153	1.014

Table S3. Selected bond lengths [Å] for FAZT-Rb and AZT-Rb.

Phase	Fe-C	Rb-N	C-N
LTP in FAZT-Rb	1.916(10)	3.145(9)	1.173(13)
	1.915(10)	2.961(8)	1.141(11)
	1.955(8)	2.971(8)	1.127(11)
	1.955(8)	3.182(8)	1.139(12)
	1.948(8)	3.083(9)	1.138(12)
	1.948(8)	3.188(9)	1.139(12)
HTP in FAZT-Rb	1.916(6)	3.030(7)	1.198(10)
LTP in AZT-Rb	1.939(8)	3.013(8)	1.145(11)
	1.939(9)	2.954(9)	1.145(13)
	1.969(9)	2.971(8)	1.150(12)
	1.969(9)	2.986(8)	1.156(12)
	1.945(9)	3.028(8)	1.168(12)
	1.945(9)	3.000(9)	1.136(13)
HTP in AZT-Rb	1.925(7)	2.957(10)	1.201(11)

Table S4. Selected bond angles [°] for FAZT-Rb and AZT-Rb.

Phase	C-Fe-C		N-Rb-N		Rb-N-C	N-C-Fe
LTP in FAZT-Rb	94.0(4)	90.2(3)	126.3(3)	71.9(2)	145.0(8)	175.2(9)
	94.0(4)	90.2(3)	76.6(3)	95.4(3)	167.7(8)	178.3(8)
	86.0(4)	89.7(4)	89.0(3)	80.0(2)	169.0(8)	179.6(8)
	86.0(4)	90.3(4)	79.4(2)	109.0(3)	153.2(8)	177.7(10)
	89.8(3)	89.7(4)	83.4(3)	84.4(2)	141.8(8)	174.8(9)
	89.8(3)	90.3(4)	91.1(3)	83.3(3)	144.1(7)	176.4(8)
HTP in FAZT-Rb	90.0		88.95(10)	91.05(10)	152.1(12)	159.9(9)
			82.3(4)	105.6(7)		
			97.7(4)	105.6(7)		
LTP in AZT-Rb	89.9(3)	93.6(3)	72.3(2)	107.7(2)	151.7(7)	178.0(8)
	93.6(3)	86.4(3)	97.3(2)	78.4(2)	166.6(8)	179.1(8)
	91.6(4)	87.0(3)	84.7(2)	87.2(2)	150.1(8)	175.9(8)
	90.1(3)	87.0(3)	99.2(2)	100.5(2)	156.7(7)	175.2(9)
	93.6(3)	93.0(3)	104.0(2)	68.0(2)	155.7(7)	178.0(8)
	86.4(3)	93.0(3)	90.6(2)	88.5(2)	145.8(8)	178.3(8)
HTP in AZT-Rb	90.000(1)		89.16(5)	103.9(4)	155.6(7)	162.6(5)
			83.08(19)	90.84(5)		
			96.92(19)	76.1(4)		

Table S5. The crystal data for compounds FAZT-K and AZT-K at different temperatures.

	$[C_3H_6NHF]_2[KFe(CN)_6]$		$[C_3H_6NH_2]_2[KFe(CN)_6]$	
Formula weight	403.26	806.52	351.15	734.55
Temperature/K	260	313	93	300
Crystal system	triclinic	cubic	tetragonal	cubic
Space group	$P\bar{1}$	$Fm\bar{3}m$	$P4_2/m$	$Fm\bar{3}m$
a/Å	8.0909(5)	11.9496(6)	8.3464(11)	11.8711(3)
b/Å	8.4371(6)	11.9496(6)	8.3464(11)	11.8711(3)
c/Å	14.3951(6)	11.9496(6)	11.807(3)	11.8711(3)
α/°	104.053(5)	90	90	90
β/°	90.862(4)	90	90	90
γ/°	118.541(7)	90	90	90
Volume/Å^3	827.45(10)	1706.3(3)	822.5(3)	1672.91(13)
Z	2	2	2	2
μ/mm^{-1}	9.878	1.160	9.693	9.534
ρ_{calc}/g ·cm^{-3}	1.619	1.570	1.418	1.458
R_{int}	0.0676	0.0128	0.0247	0.0064
R_1 [I>=2σ (I)]	0.0903	0.0348	0.1240	0.0372
wR_2 [I>=2σ (I)]	0.2402	0.1176	0.2921	0.0812
R_1 [all data]	0.1103	0.0356	0.1311	0.0372
wR_2 [all data]	0.2587	0.1216	0.2970	0.0812
Goodness-of-fit on F^2	1.091	0.923	1.095	1.076

Table S6. Selected bond lengths [Å] for FAZT-K and AZT-K.

Phase	Fe-C	K-N		C-N
LTP in FAZT-K	1.941(5)	2.845(6)		1.159(8)
	1.946(6)	3.077(6)		1.144(7)
	1.948(6)	3.066(6)		1.149(7)
	1.948(6)	2.955(5)		1.165(8)
	1.948(5)	2.851(5)		1.145(8)
	1.949(5)	3.053(6)		1.143(8)
HTP in FAZT-K	1.937(5)	2.931(5)		1.178(8)
LTP in AZT-K	1.939(15)	3.003(19)	2.86(2)	1.08(2)
	1.867(15)	2.888(14)	2.86(2)	1.025(17)
	2.001(14)	2.888(14)	3.003(19)	1.10(2)
HTP in AZT-K	1.940(4)	2.882(5)		1.174(7)

Table S7. Selected bond angles [°] for FAZT-K and AZT-K.

Phase	C-Fe-C		N-K-N		K-N-C	N-C-Fe
LTP in FAZT-K	92.8(2)	91.5(2)	78.10(16)	91.71(17)	158.8(5)	176.9(5)
	87.2(2)	88.5(2)	83.68(16)	82.02(17)	146.8(5)	177.3(5)
	87.2(2)	93.5(2)	84.49(16)	124.77(17)	169.2(5)	179.2(5)
	92.8(2)	86.5(2)	108.54(16)	83.11(17)	170.4(5)	174.7(5)
	88.5(2)	86.5(2)	73.29(17)	90.81(18)	146.3(5)	175.6(6
	91.5(2)	93.5(2)	93.29(17)	77.06(17)	120.4(4)	177.5(5)
HTP in FAZT-K	90.0		89.21(7)	103.5(6)	156.3(10)	163.0(7)
			83.3(3)	96.7(3)		
			90.79(7)	76.5(6)		
LTP in AZT-K	90.00(1)	90.00(2)	90.00(1)	90	180.0	180.0
	90.00(1)	90.00(2)	90.00(1)	90.00(1)		
	90.00(1)	82.4(5)	90.00(1)	79.8(4)	161.9(14)	172.5(15)
	90.00(1)	82.4(5)	90.00(1)	100.2(4)		
	90.00(1)	97.6(5)	90	79.8(4)	173.4(13)	179.4(13)
	90.00(1)	97.6(5)	90.00(1)	100.2(4)		
HTP in AZT-K	90.000(1)		89.999(1)	83.8(2)	158.4(7)	164.6(5)
			102.4(4)	90.001(1)		
			90.67(5)	89.33(5)		

Table S8. The crystal data for compounds FAZT-Cs and AZT-Cs at different temperatures.

	$[C_3H_6NHF]_2[CsFe(CN)_6]$			$[C_3H_6NH_2]_2[CsFe(CN)_6]$	
Formula weight	497.07	497.07	994.14	461.09	461.09
Temperature/K	300	388	413	298	323
Crystal system	triclinic	monoclinic	cubic	monoclinic	cubic
Space group	$P\bar{1}$	C_2/c	$Fm\bar{3}m$	$P2_1/c$	$Fm\bar{3}m$
a/Å	8.29732(17)	15.1525(8)	12.2916(5)	14.3722(10)	12.2181(7)
b/Å	8.5989(2)	8.2653(3)	12.2916(5)	8.6742(4)	12.2181(7)
c/Å	15.0572(3)	15.3801(5)	12.2916(5)	15.0692(8)	12.2181(7)
α/°	105.1112(19)	90	90	90	90
β/°	90.3127(16)	107.358(4)	90	109.484(7)	90
γ/°	118.838(2)	90	90	90	90
Volume/Å^3	897.53(4)	1838.48(14)	1857.1(2)	1771.05(19)	1823.9(3)
Z	2	4	2	4	4
μ/mm^{-1}	2.869	2.802	2.774	22.692	22.034
ρ_{calc}/g ·cm^{-3}	1.839	1.796	1.778	1.729	1.679
R_{int}	0.0151	0.0280	0.0098	0.0799	0.0567
R_1 [I>=2σ (I)]	0.0211	0.0342	0.0317	0.0881	0.0404
wR_2 [I>=2σ (I)]	0.0557	0.1012	0.0919	0.2189	0.1179
R_1 [all data]	0.0229	0.0369	0.0344	0.1206	0.0421
wR_2 [all data]	0.0567	0.1100	0.0976	0.2475	0.1191
Goodness-of-fit on F^2	1.033	1.139	0.976	1.072	1.125

Table S9. Selected bond lengths [Å] for FAZT-Cs and AZT-Cs.

Phase	Fe-C	Cs-N	C-N
LTP in FAZT-Cs	1.9364(18)	3.2725(18)	1.146(2)
	1.9435(18)	3.3096(19)	1.150(2)
	1.9423(19)	3.3260(18)	1.150(3)
	1.9423(19)	3.2894(19)	1.142(3)
	1.9398(19)	3.1142(19)	1.143(3)
	1.9398(19)	3.1240(19)	1.147(2)
ITP in FAZT-Cs	1.944(3)	3.303(3)	1.134(4)
	1.944(3)	3.303(3)	1.139(4)
	1.935(3)	3.140(9)	1.157(9)
	1.935(3)	3.140(10)	
	1.935(3)	3.228(3)	1.15(3)
	1.935(3)	3.228(3)	
HTP in FAZT-Cs	1.904(8)	3.177(11)	1.209(15)
LTP in AZT-Cs	1.942(9)	3.141(8)	1.147(11)
	1.942(9)	3.175(8)	1.145(11)
	1.946(8)	3.203(9)	1.142(13)
	1.936(9)	3.240(8)	1.154(11)
	1.945(10)	3.138(11)	1.141(11)
	1.945(10)	3.214(8)	1.149(14)
HTP in AZT-Cs	1.893(17)	3.15(2)	1.24(3)

Table S10. Selected bond angles [°] for FAZT-Cs and AZT-Cs.

Phase	C-Fe-C		N-Cs-N		Cs-N-C	N-C-Fe
LTP in FAZT-Cs	91.25(8)	90.25(9)	85.93(5)	99.22(6)	137.89(15)	175.84(17)
	88.75(8)	89.75(8)	81.32(5)	89.46(6)	144.06(17)	177.95(19)
	91.25(8)	93.10(8)	109.88(5)	87.12(7)	140.39(16)	178.6(2)
	88.75(8)	86.90(8)	83.06(5)	82.37(6)	142.71(17)	175.56(18)
	90.25(9)	93.10(8)	127.75(5)	74.84(6)	167.27(19)	176.92(17)
	89.75(9)	86.90(8)	69.74(6)	77.84(6)	161.8(2)	177.8(2)
ITP in FAZT-Cs	89.40(12)	93.10(12)	128.62(14)	104.66(12)	140.5(3)	175.2(3)
	90.60(12)	86.90(12)	80.6(7)	71.6(7)		
	89.40(12)	88.38(14)	80.6(7)	71.6(7)	152.2(4)	171.7(13)
	90.60(12)	91.62(14)	83.1(6)	87.5(7)		
	86.90(12)	88.37(14)	104.66(12)	87.5(7)	140(3)	175.3(4)
	93.10(12)	91.63(14)	86.77(11)	75.4(14)	172.4(9)	161(2)
HTP in FAZT- Cs	90.000(2)		91.39(15)	72.1(10)	146.9(17)	155.8(12)
			88.61(15)	107.9(10)		
			81.2(5)	98.8(5)		
LTP in AZT- Cs	91.9(4)	91.7(4)	112.2(2)	65.8(2)	144.8(8)	177.6(8)
	91.9(4)	91.7(4)	103.5(3)	100.8(3)	136.0(8)	179.0(10)
	88.1(4)	89.0(4)	85.6(2)	82.7(3)	150.5(8)	177.0(8)
	88.1(4)	89.0(4)	76.8(2)	105.9(3)	165.4(10)	178.6(9)
	88.3(4)	91.0(4)	88.3(2)	96.2(3)	150.2(8)	172.9(9)
	88.3(4)	91.0(4)	88.6(2)	71.4(2)	152.3(8)	175.4(9)
HTP in AZT- Cs	90.0		91.6(3)	90.000(3)	145(3)	154(2)
			109.5(17)	80.4(8)		
			88.4(3)	99.6(8)		

References:

1. X. Zhang, X.-D. Shao, S.-C. Li, Y. Cai, Y.-F. Yao, R.-G. Xiong and W. Zhang, *Chem. Commun.*, 2015, **51**, 4568-4571.
2. R.-G. Qiu, X.-X. Chen, R.-K. Huang, D.-D. Zhou, W.-J. Xu, W.-X. Zhang and X.-M. Chen, *Chem. Commun.*, 2020, **56**, 5488-5491.

3. M. Rok, G. Bator, B. Zarychta, B. Dziuk, D. K. Skałecki, W. Medycki and M. Zamponi, *Cryst. Growth Des.*, 2019, **19**, 4526-4537.
4. W.-J. Xu, K.-P. Xie, Z.-F. Xiao, W.-X. Zhang and X.-M. Chen, *Cryst. Growth Des.*, 2016, **16**, 7212-7217.
5. M. Rok, M. Moskwa, M. Działowa, A. Bieńko, C. Rajnák, R. Boča and G. Bator, *Dalton Trans.*, 2019, **48**, 16650-16660.
6. M. Rok, B. Zarychta, M. Moskwa, B. Dziuk, W. Medycki and G. Bator, *Dalton Trans.*, 2020, **49**, 1830-1838.
7. X. Liu, L. Li, Y.-Z. Yang and K.-L. Huang, *Dalton Trans.*, 2014, **43**, 4086-4092.
8. W.-J. Xu, S.-L. Chen, Z.-T. Hu, R.-B. Lin, Y.-J. Su, W.-X. Zhang and X.-M. Chen, *Dalton Trans.*, 2016, **45**, 4224-4229.
9. M. Rok, J. K. Prytys, V. Kinzhybalo and G. Bator, *Dalton Trans.*, 2017, **46**, 2322-2331.
10. Y.-X. Li, X.-L. Wang, Y. Li, O. Sato, Z.-S. Yao and J. Tao, *Inorg. Chem.*, 2020, **60**, 380-386.
11. C. Shi, X.-B. Han, Y. Wang and W. Zhang, *Inorg. Chem. Front.*, 2016, **3**, 1604-1608.
12. W.-J. Xu, K. Romanyuk, J. M. G. Martinho, Y. Zeng, X.-W. Zhang, A. Ushakov, V. Shur, W.-X. Zhang, X.-M. Chen, A. Kholkin and J. Rocha, *J. Am. Chem. Soc.*, 2020, **142**, 16990-16998.
13. W. Zhang, H.-Y. Ye, R. Graf, H. W. Spiess, Y.-F. Yao, R.-Q. Zhu and R.-G. Xiong, *J. Am. Chem. Soc.*, 2013, **135**, 5230-5233.
14. W.-J. Xu, P.-F. Li, Y.-Y. Tang, W.-X. Zhang, R.-G. Xiong and X.-M. Chen, *J. Am. Chem. Soc.*, 2017, **139**, 6369-6375.
15. M. Rok, A. Ciżman, B. Zarychta, J. K. Zaręba, M. Trzebiatowska, M. Mączka, A. Stroppa, S. Yuan, A. E. Phillips and G. Bator, *J. Mater. Chem. C*, 2020, **8**, 17491-17501.
16. Z.-X. Gong, Q.-W. Wang, J.-J. Ma, J.-Y. Jiang, D.-Y. E, Z.-Q. Li, F.-W. Qi and H. Liang, *Mat. Chem. Front.*, 2020, **4**, 918-923.